Full Title: Enhanced phase-amplitude coupling of human electrocorticography selectively in the posterior cortical region during rapid eye movement sleep

Brief running Title: Phase-amplitude coupling during sleep and wakefulness

Authors names and affiliations: Jumpei Togawa[1, 2], *Riki Matsumoto[1, 3], Kiyohide Usami[4], Masao Matsuhashi[4], Morito Inouchi[4, 5], Katsuya Kobayashi[1], Takefumi Hitomi[6], Takuro Nakae[7, 8], Akihiro Shimotake[1], Yukihiro Yamao[7], Takayuki Kikuchi[7], Kazumichi Yoshida[7], Takeharu Kunieda[9], Susumu Miyamoto[7], Ryosuke Takahashi[1] and *Akio Ikeda[4]

[1]Department of Neurology, Kyoto University Graduate School of Medicine, Kyoto, 606-8507, Japan

[2]Department of Respiratory Care and Sleep Control Medicine, Kyoto University Graduate School of Medicine, Kyoto, 606-8507, Japan

[3]Divison of Neurology, Kobe University Graduate School of Medicine, Kobe, 650-0017, Japan

[4]Department of Epilepsy, Movement Disorders and Physiology, Kyoto University Graduate

18 School of Medicine, Kyoto, 606-8507, Japan

19 [5]Department of Neurology, National Hospital Organization Kyoto Medical Center, Kyoto,

20 612-8555, Japan

21 [6]Department of Clinical Laboratory Medicine, Kyoto University Graduate School of

22 Medicine, Kyoto, 606-8507, Japan

23 [7]Department of Neurosurgery, Kyoto University Graduate School of Medicine, Kyoto, 606-

24 8507, Japan

25 [8]Department of Neurosurgery, Shiga General Hospital, Moriyama, 524-8524, Japan

26 [9]Department of Neurosurgery, Ehime University Graduate School of Medicine, Ehime, 791-

27 0295, Japan

28

29 ***Correspondence to:**

30 Riki Matsumoto

31 Division of Neurology, Kobe University Graduate School of Medicine, Kobe, Japan

32 matsumot@med.kobe-u.ac.jp

7-5-1 Kusunoki-cho, Chuo-ku, Kobe, Japan 650-0017

Tel: +81-(0)78-382-5885

Fax: +81-(0)78-382-5899

&

Akio Ikeda

Department of Epilepsy, Movement Disorders and Physiology, Kyoto University Graduate School of Medicine, Kyoto, Japan

akio@kuhp.kyoto-u.ac.jp

54 Shogoin-Kawahara-cho, Sakyo-ku, Kyoto 606-8507, Japan

Tel: +81-(0)75-751-3318

Fax: +81-(0)75-751-3663

This is a pre-copyedited, author-produced version of an article accepted for publication in Cerebral Cortex following peer review. There is a title change between the accepted manuscript and the version of record, and the title of this manuscript is the same as the version of record. The version of record (Cereb Cortex. 2022 Mar 15: bhac079.) is available online at: https://doi.org/10.1093/cercor/bhac079 (doi:10.1093/cercor/bhac079)

50

Abstract

The spatiotemporal dynamics of interaction between slow (delta or infraslow) waves and fast (gamma) activities during wakefulness and sleep are yet to be elucidated in human electrocorticography (ECoG). We evaluated phase-amplitude coupling (PAC), which reflects neuronal coding in information processing, using ECoG in 11 patients with intractable focal epilepsy. PAC was observed between slow waves of 0.5-0.6 Hz and gamma activities, not only during light sleep and slow wave sleep (SWS), but even during wakefulness and rapid eye movement (REM) sleep. While PAC was high over a large region during SWS, it was particularly strong in the posterior cortical region around the temporoparietal junction during REM sleep. PAC tended to be higher in the posterior cortical region than in the frontal cortical region (lateral frontal lobe except for precentral gyrus) even during wakefulness. Our findings suggest that the posterior cortical region has a functional role in REM sleep and may contribute to the maintenance of the dreaming experience.

Keywords: consciousness, electrocorticography, phase-amplitude coupling, REM sleep, wakefulness

Understanding the neuronal mechanisms of human consciousness is one of the most fundamental challenges in the field of neuroscience (Koch *et al.* 2016; Mashour 2018). The study of human sleep can help in understanding these mechanisms (Hobson 2009; Koch *et al.* 2016; Boly *et al.* 2017). During sleep, consciousness fades, but dreams occur, particularly during rapid eye movement (REM) sleep (Aserinsky and Kleitman 1953). REM sleep is considered to be an activated brain state, at least partly similar to wakefulness, and may provide clues to the neural correlates of consciousness (Hobson 2009).

The electrophysiological features of sleep have been intensively investigated over recent decades. Non-REM (NREM) sleep represents a deep sleep level and contains slow oscillations in the low frequency range (<1 Hz) (Timofeev 2000; Dalal *et al.* 2010; Le Van Quyen *et al.* 2010; Nir *et al.* 2011). Conversely, REM sleep shows activated and desynchronized electroencephalography (EEG) patterns, similar to wakefulness (Aserinsky and Kleitman 1953; Steriade *et al.* 2001). Global cerebral blood flow reportedly increases during REM sleep, compared with that in NREM sleep (Braun 1997). A recent study showed that dreaming was associated with local decreases in scalp EEG delta activity in posterior cortical regions (Siclari *et al.* 2017), which were suggested to be the regions to which neural

correlates of dreaming are restricted. The temporo-parietal-occipital region, involving multisensory integration, is called a posterior "hot zone" and is thought to be a candidate of neural correlates of consciousness (Koch *et al.* 2016).

Oscillations of electrical brain activity reflect rhythmic changes in cortical excitability (Fries 2005). While high-frequency brain activity, i.e., high gamma activity, is thought to reflect local neuronal firing and cortical processing, low-frequency brain rhythms, i.e., delta waves or infraslow waves, are entrained across distributed brain regions (von Stein and Sarnthein 2000; Buzsaki and Wang 2012). Recently, an interaction of different frequency bands known as cross-frequency coupling (CFC) is believed to represent the transfer of information from spatially large brain networks to local cortical domains in the brain (Canolty and Knight 2010). Phase-amplitude coupling (PAC) is a form of CFC that represents the interaction of the phase of a slower rhythm and the amplitude of a faster rhythm (Tort *et al.* 2010). The strength of PAC increases during behavioral events and correlates with learning performance; hence, it is thought to play physiological roles in information processing (e.g., visual, auditory, and memory) and transfer in the brain (Canolty *et al.* 2006; Tort 2008; Handel and Haarmeier 2009; Tort *et al.* 2009; Axmacher *et al.* 2010; Canolty and Knight 2010; Fontolan *et al.* 2014). Previous studies have shown that PAC

between delta and gamma activities is enhanced during slow wave sleep (SWS) (Valderrama *et al.* 2012; Takeuchi *et al.* 2015; Amiri *et al.* 2016; Nonoda *et al.* 2016; von Ellenrieder *et al.* 2020), whereas more extensive PAC is observed during wakefulness than during SWS when a wider frequency range is investigated (amplitude: 1-200 Hz, phase: 1-20 Hz) (He *et al.* 2010), suggesting the physiological roles of PAC during wakefulness. Motoi *et al*. studied the interictal PAC of slow waves (3-4 Hz) and high-frequency activity (>150 Hz), which, to the best of our knowledge, is the only study that has investigated the spatial distribution of PAC of human intracranial EEG during each sleep stage (Motoi *et al.* 2018). However, their study sought to evaluate PAC as a predictive marker for epilepsy surgery outcomes and did not focus on the slower brain oscillations. To date, the spatial dynamics of PAC between slow oscillation (delta or infraslow waves) and fast activity during each sleep stage have not been studied in detail using human intracranial EEG.

In the present study, we hypothesized that information processing and transfer in the brain are enhanced with PAC in the posterior hot zone during wakefulness and REM sleep. We aimed to investigate the spatial distribution of PAC strength using electrocorticography (ECoG) in humans.

Materials and Methods

Patients and ECoG acquisition

Of the 34 consecutive patients who underwent chronic subdural electrode implantation for presurgical evaluation of intractable focal epilepsy between June 2010 and April 2017 at our hospital, 11 patients (age 17–44 years, male: 7, female: 4) were included in the study (Table 1). The protocol adhered to the tenets of the Declaration of Helsinki and was approved by the Ethics Committee of our institute (R0603). Patient demographics are shown in Table 1 based on the classification of pathological findings and seizure outcomes described in previous papers (Wieser *et al.* 2001; Palmini *et al.* 2004).

136

Patient No.	Age Sex	Sampled hemisphere	Clinical classification	MRI lesion	Pathology	Electrodes implanted	Electrodes analyzed	Seizure Outcome	ECoG length (s)	AED
1	22 F	Bi	R FLE	-	FCD IA	52	33	1	258	CBZ, PHT
2	44 M	R	R FLE	+	mixed oligoastrocytoma/ FCD IA	48	39	1	540	CBZ, VPA, LEV, TPM
3	34 M	R	R PLE/TLE	+	posttraumatic change, scar, HS	82	57	2	324	TPM, ZNS, CBZ, LEV
4	28 F	R	R PLE	+	low grade glioma	56	31	1	606	LEV, CBZ, CZP
5	39 M	L	L FLE	+	FCD IIB	148	32	1	120	LEV, CBZ
6	39 M	R	R TLE	+	FCD IA/HS	90	63	1	342	VPA, CBZ, CLB, fosPHT
7	29 M	R	R FLE	-	FCD IA	112	60	4	136	LEV, CBZ, LTG
8	21 M	L	L TLE	+	FCD IA/HS	82	39	1	102	LEV, CLB
9	17 F	L	L FLE	+	DNT	92	71	1	450	LEV, fosPHT
10	23 F	L	R PLE	-	FCD IIB	84	49	1	468	LEV, CBZ, CLB, fosPHT
11	34 M	L	L TLE	+	FCD IA/HS (clinically diagnosed)	102	62	3	167	CBZ, LTG, fosPHT

137

138 **Table 1. Patient demographics and clinical information**

139 Seizure outcomes are based on criteria proposed by the International League Against Epilepsy (Wieser *et al.* 2001). Pathological findings are

140 based on a classification proposed in a previous paper. (Palmini *et al.* 2004). AED that was administered on the day of ECoG recording is

141 indicated.

142

143 **Abbreviations** F: female M: male Bi: bilateral R: right L: left FLE: frontal lobe epilepsy TLE: temporal lobe epilepsy PLE: parietal lobe

144 epilepsy FCD: focal cortical dysplasia HS: hippocampal sclerosis DNT: dysmorphic neuroepithelial tumor AED: anti-epileptic drug CBZ:

145 carbamazepine PHT: phenytoin VPA: valproic acid LEV: levetiracetam TPM: topiramate ZNS: zonisamide CZP: clonazepam CLB: clobazam

146 fosPHT: fosphenytoin LTG: lamotrigine

The ECoG acquisition procedure is described in detail elsewhere (Usami *et al.*, 2015). Subdural platinum electrodes (AD-TECH, Oak Creek, WI, USA) had a recording diameter of 2.3 mm and were placed with an interelectrode distance of 10 mm. Grid electrodes (Unique Medical, Tokyo, Japan) with a recording diameter of 3 mm and center-to-center interelectrode distance of 5 mm were additionally used in one patient (patient 4). In another patient (patient 5), grid electrodes (Unique Medical) with a recording diameter of 3 mm and center-to-center interelectrode distance of 10 mm, as well as grid electrodes with a recording diameter of 1.5 mm and center-to-center interelectrode distance of 5 mm, were also used. ECoG was recorded using EEG1100 (Nihon Koden, Tokyo, Japan) for patients 1–9 and EEG1200 (Nihon Koden) for patients 10 and 11, under the following two conditions: (1) band-pass filter 0.016–600 Hz and sampling rate 2000 Hz (patients 2, 4, 5, 8, 10, and 11) and (2) band-pass filter 0.016–300 Hz and sampling rate 1000 Hz (patients 1, 3, 5, 6, 7, and 9). ECoG was referenced to a scalp electrode placed on the skin over the mastoid process, contralateral to the side of electrode implantation, except for patient 6, whose ECoG was referenced to an electrode on the galea because of motion artifacts in the mastoid electrode. The total number of implanted intracranial electrodes was 948 for the 11 patients. Depth

electrodes implanted in patients 4, 5, and 7 (60 in total) were excluded, and only subdural electrodes were included. Sixty-one electrodes in patient 5 and 28 electrodes in patient 8 were not available for this study, since a higher sampling rate (2000 Hz) was adopted for sleep research, which limited the numbers of electrodes available for recording.

Original ECoG data were reviewed by two board-certificated electroencephalographers (JT and MI), and three electrodes contaminated with artifacts were excluded. The seizure onset zone (SOZ) and irritative zone (IZ) were determined by reviewing clinical records. The SOZ was defined as the electrode-containing area to which conventional EEG change spreads within 5 s from the earliest onset. The IZ was defined as the electrode-containing area with interictal epileptic spikes. Electrodes within the SOZ and/or IZ (260 in total) were excluded from this study, leaving 536 residual electrodes for inclusion. All patients had both SOZs and IZs, except for patient 5, who had no seizure during the period of intracranial electrode implantation. ECoG was recorded through at least one night, with additional scalp electrodes, electrooculogram, and chin electromyogram for sleep staging. According to the standard Rechtschaffen & Kales sleep-staging criteria (Rechtschaffen and Kales 1968), sleep stages (wakefulness, light sleep [LS], SWS, and REM sleep) were defined. Awake ECoG data of patient 5 were not available because of

occasional artifactual signals; therefore, awake data were analyzed using the data of the other 10 patients (504 electrodes). In the statistical analysis using regions of interest (ROIs), the data of patient 5 were excluded from analysis in all sleep stages.

ECoG data obtained within 150 min after focal onset aware/impaired awareness seizures or within 24 h after generalized tonic-clonic seizures were excluded. To avoid contamination by artifactual signals, we carefully checked the raw ECoG waveforms visually and eliminated segments that were contaminated by artifactual signals and those that were at 1 second margins of the contaminated segments. The ECoG data for the four sleep stages for a patient were maintained at the same length (102–606 s).

Image processing

The method for standard electrode placement and coregistration to the Montreal Neurological Institute (MNI) standard space has been reported in detail previously (Matsumoto *et al.* 2004; Matsumoto *et al.* 2011). In brief, anatomic T1-weighted volume data (voxel size: 0.9 mm × 0.9 mm × 0.9 mm), using magnetization-prepared rapid gradient echo sequences, were obtained before and after subdural electrode implantation. Using magnetic resonance imaging after implantation, we identified the electrode location by confirming a signal void due to the

properties of the platinum alloy electrode. The coordinates of electrodes of all patients were then linearly coregistered to the scan image obtained before implantation, and thereafter non-linearly warped to MNI standard space using FNIRT (www.fmrib.ox.ac.uk/fsl/fnirt). The electrodes on the right hemisphere were flipped to the left hemisphere for group analysis (Fig. 1A).

Experimental Design and Statistical Analysis

PAC calculation and all statistical analyses were performed using MATLAB 2015a (Mathworks, Natick, MA, USA).

PAC calculation

We adopted an index, the correlation coefficient (CC), which was similar to the Modulation Index (MI) described previously (Canolty *et al.* 2006). The CC differed from the MI in that we calculated the CC of the instantaneous amplitude of fast activity and the instantaneous phase of slow waves, instead of the temporal mean of the product of these two values. We also normalized it to surrogate distribution, which was generated from randomly time-shifted data, instead of mean and standard deviation, since the absolute value of surrogate CC

(surCC) data did not necessarily follow a normal distribution in our data set (Supplementary Fig. S1).

Therefore, we calculated PAC as follows: Instantaneous amplitude of fast activity and the instantaneous phase of slow waves were calculated using Hilbert transformation. Then, the CC between instantaneous amplitude and instantaneous phase was calculated as follows:

$$\mathrm{CC} = \sum_{j=1}^{N}\left(\mathrm{AF}(t_j)\,\overline{e^{i\varphi S(t_j)}}\right) / \sqrt{\left\{\sum_{j=1}^{N}\left(|\mathrm{AF}(t_j)|^2\right)\right\}\left\{\sum_{j=1}^{N}\left(|(e^{i\varphi S(t_j)})|^2\right)\right\}}$$

where t_j is the sampled time of sample j, $\mathrm{AF}(t_j)$ is the instantaneous amplitude of fast activity, $\varphi S(t_j)$ is the instantaneous phase of slow wave, and N is the number of samples. Overline notation indicates a complex conjugate. The absolute value of CC (aCC) was then calculated.

For statistical analysis, randomly time-shifted instantaneous amplitude and instantaneous phase data were generated as surrogate data, and the absolute values of surCC were calculated 10,000 times. Using the distribution of the absolute values of surCC, the original aCC was converted to a p-value and then transformed to a z-value using inverse normal cumulative distribution function. This was termed “PAC-Z” and regarded as a marker of PAC strength in this study.

Statistical analysis of PAC-Z in each patient

In each patient, PAC-Z was calculated in all combinations of “bins of fast frequency” × “bins of slow wave frequency” in all channels. To test the statistical significance, the threshold was corrected for multiple comparisons using a false discovery rate of 0.05 in each patient. Only clusters of bins that contained more than four contiguous bins within a channel were regarded as significant. The PAC-positive rate was calculated in each combination of a bin of slow wave frequency and a bin of fast activity frequency, as a quotient of the number of PAC-positive channels divided by the total number of channels.

PAC with wide frequency range

PAC is reportedly enhanced between the phase of delta waves and the amplitude of gamma activities during SWS (Valderrama *et al.* 2012; Takeuchi *et al.* 2015; Amiri *et al.* 2016; Nonoda *et al.* 2016; von Ellenrieder *et al.* 2020). However, while previous studies have analyzed PAC to a few frequency bands for amplitude (fast activities), the difference among frequency bands for phase (slow waves) has not been tested in detail. Therefore, we calculated PAC strengths using the phases of a wide range of slow wave frequencies with small bins to determine the frequency ranges targeted in this study. Fast activity frequency

was divided into comparatively large bins for the sake of computation load. Slow wave frequency was divided into 20 bins, with 1.0516-Hz steps (central frequency: 0.02–20 Hz) and fast activity frequency was divided into 5 bins with 37.5-Hz steps (central frequency: 20–170 Hz). Averaged PAC-Zs and PAC-positive rates among all analyzed electrodes were then calculated (Supplementary Fig. S2).

PAC with narrow frequency range

Based on the results of PAC analysis with wide frequency range, we focused on a narrower frequency range that showed comparatively high PAC (Supplementary Fig. S3). The lower slow wave frequency range (<2 Hz) was divided into 15 bins in 0.1415-Hz steps (central frequency: 0.02–2 Hz), while fast activity frequency was divided into four bins in 40-Hz steps (central frequency: 50–170 Hz). PAC-Z was calculated for each pair of slow wave and fast activity frequency bins using the same procedure as in the wide range frequency analysis (Supplementary Fig. S3).

PAC-Z strength map

Using the method employed in our previous study (Nakae *et al.* 2020), we projected PAC-Z

266 to MNI standard space (Supplementary Fig. S4 and Fig. 2). PAC-Z was calculated for each
267 channel within the ranges of frequency described above (15 slow wave frequency bins × four
268 fast activity frequency bins). The four PAC-Zs of the fast activity frequency bins were
269 averaged for each slow wave frequency bin. Thus, each channel had 15 PAC-Z values per
270 stage. Then, we plotted PAC-Z into the nearest-neighbor voxel of each electrode and applied
271 spatial smoothing with a Gaussian kernel (full-width at half-maximum: 14 mm, kernel size:
272 30 mm). We made an electrode-density map in the same manner, plotting the value of 1
273 instead of the PAC-Z. In the area where electrodes were placed closely, a voxel might have a
274 value more than 1 in this map. Then, the PAC-Z map was divided by the electrode-density
275 map, voxel-by-voxel, to avoid bias due to electrode density, and only voxels for which there
276 were more than three electrodes within a 15-mm radius were colored.
277
278 **Anatomical ROIs**
279 We delineated two anatomical ROIs, the frontal ROI and posterior ROI, to compare the
280 averaged PAC-Zs of channels in the frontal and posterior cortical regions, respectively. We
281 used the temporoparietal junction (TPJ) as the posterior ROI, because this region reportedly
282 integrates multisensory input and generates the feeling of bodily self-consciousness (Eddy

283 2016; Grivaz *et al.* 2017). Although there is limited consensus regarding the anatomical

284 definition of the TPJ, we made a TPJ ROI based on "TPJ-related fields in probabilistic

285 atlases," described in a previous paper (Schurz *et al.* 2017). The posterior ROI in our study

286 was made by combining the lateral occipital cortex superior division, angular gyrus,

287 supramarginal gyrus posterior division, and middle temporal gyrus temporo-occipital part in

288 the Oxford-Harvard atlas in FSL (www.fmrib.ox.ac.uk/fsl). As a control, the frontal ROI was

289 made to include the whole lateral frontal lobe, except for the precentral gyrus using the same

290 atlas. We excluded the precentral gyrus from the frontal ROI because it forms part of the

291 primary motor cortex and, therefore, is likely to be functionally different from other frontal

292 regions (Wood and Grafman 2003). Both ROIs were limited to the voxels for which more

293 than three patients' electrodes were placed within a 15-mm radius (Fig. 3A; Green lines are

294 the edges without this limitation). The frontal ROI included 147 electrodes, while the

295 posterior ROI included 50 electrodes.

296

297 **Statistical analysis of PAC-Z values in two ROIs**

298 First, all electrodes included in each frontal and posterior ROI were extracted. Second, four

299 PAC-Z values of fast activity frequency bins (central frequency: 50, 90, 130, and 170 Hz)

were averaged in each slow wave frequency bin in each channel. Third, the PAC-Z values in two bins of slow wave frequencies (0.44 and 0.59 Hz) were extracted and averaged to generate the PAC-Z of the channel. We chose these two bins because PAC tended to be high around a slow wave frequency of approximately 0.5 Hz. PAC-Z values calculated in this manner were labeled as the PAC-Z values of each channel. Accordingly, each channel had one PAC-Z value for each sleep stage. Averaged PAC-Z values during each sleep stage were plotted (Fig. 3B). To compare the PAC-Z values of the frontal and posterior ROIs, we used Mann-Whitey U test within each stage, since our PAC-Z data did not necessarily follow a normal distribution in our preliminary analysis. Multiple comparisons were performed using Bonferroni's correction.

Power spectrum of slow wave and fast activity

To investigate whether the frequency bands of slow wave and fast activity that showed high PAC-Z had higher power than other frequency bands, we analyzed the power spectrum of slow wave and fast activity. The power spectral density of ECoG was calculated using discrete Fourier transform. Common logarithmic power was calculated at each electrode and was averaged over all electrodes (Supplementary Fig. S5).

Power distribution map and analysis with ROIs

To confirm that PAC strength distribution was not determined only by the power of slow wave and fast activity, we projected the power of slow wave and fast activity to MNI standard space (Supplementary Fig. S6 and S7). We converted logarithmic power to z-values among all electrodes in each sleep stage and for each combination of frequency band bins, and then applied the same method that we used to prepare the PAC strength map but using the z-value of logarithmic power instead of the PAC-Z value.

We also performed analyses with anatomical ROIs using logarithmic power data instead of PAC-Z values. Supplementary Figures S8 and S9 show the averaged logarithmic power in each frontal and posterior ROI plotted in each sleep stage. To compare the averaged logarithmic power in the frontal and posterior ROIs, we used the averaged logarithmic power of two bins (0.45 and 0.59 Hz) for slow waves and all four bins for fast activity (central frequency: 50, 90, 130, 170 Hz). We performed the Mann-Whitey U test in each sleep stage. Multiple comparisons were corrected using Bonferroni's method.

Data availability

The data that support the findings of this study are available from the corresponding author upon reasonable request.

Results

PAC was observed in original ECoG waveforms. Ahead of mathematical analysis, we examined ECoG waveforms to confirm that PAC was a real phenomenon occurring in the brain and not a computational artifact. Figure 1A shows all non-epileptic electrodes transferred to the MNI standard space and two representative ECoG waveforms from a patient with chronic subdural electrode implantation for presurgical evaluation of intractable focal epilepsy (patient 2 in Table 1). During both SWS and REM sleep, gamma activity increased specifically around delta activity (Fig. 1B and 1C).

Figure 1

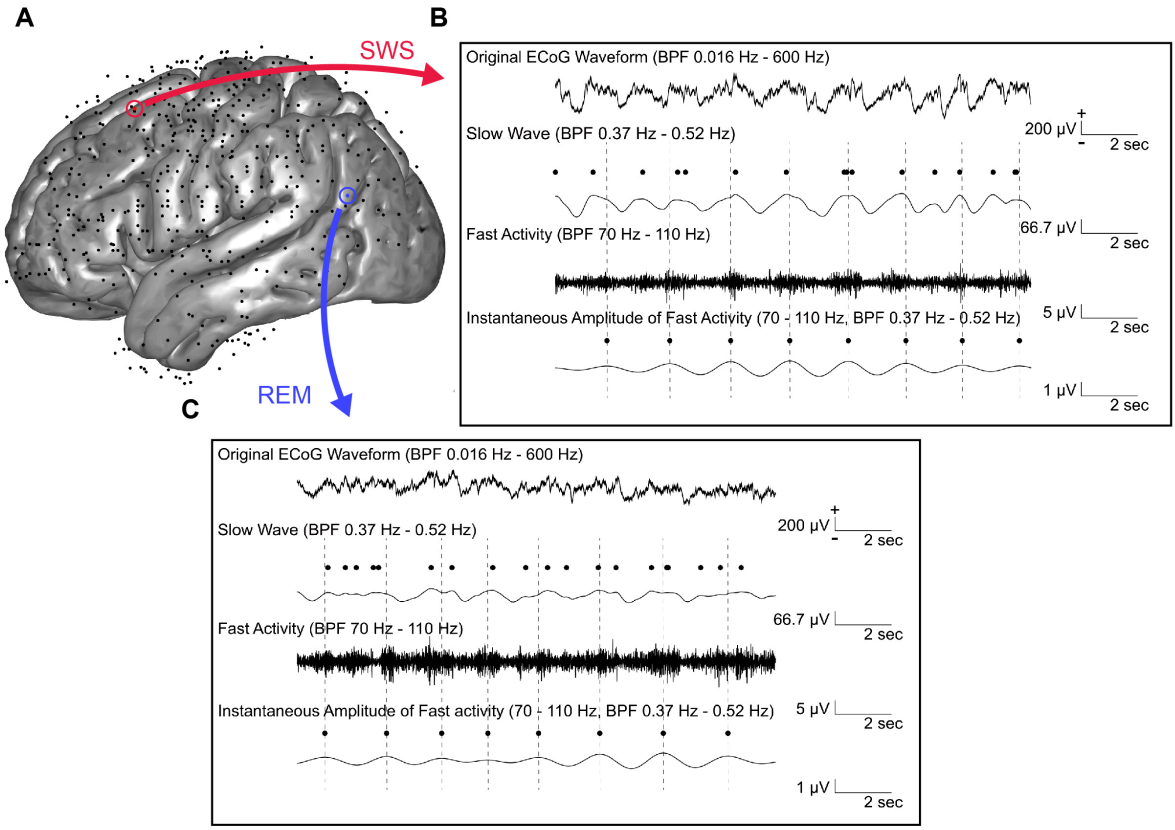

Representative electrocorticography (ECoG) waveforms in different sleep stages. ECoG is recorded during at least one night and classified into four stages (wakefulness, light sleep, slow wave sleep [SWS], and rapid eye movement [REM] sleep) **A**) Subdural electrodes in non-epileptic areas in all patients (N = 11, a total of 536 electrodes) are coregistered to MNI standard space. **B**) Waveforms sampled from a channel of patient 2 in the frontal region during SWS and **C)** in the posterior region during REM sleep. Original ECoG waveform (band-pass filter [BPF]: 0.0016–600 Hz), slow wave (BPF: 0.37–0.52 Hz), fast activity (BPF: 70–110 Hz), and instantaneous amplitude of fast activity (BPF: 70–110 Hz) are shown. Instantaneous amplitude is band-pass filtered (0.37–0.52 Hz) for presentation. Frequency

bands of slow wave and fast activity are chosen as representative examples of phase-amplitude coupling (PAC). Note that averaged values of multiple bins are used in the later analysis. Positive peaks of slow waves and instantaneous amplitudes of fast activity are indicated by dots. Vertical broken lines are drawn over positive peaks of instantaneous amplitudes of fast activity to show the phase similarity of these two waveforms. During both SWS and REM sleep, gamma activity increases specifically around delta activity.

Central frequency of PAC increase was 0.5-0.6 Hz in slow waves during all sleep stages.

First, we analyzed PAC for wide frequency range (central frequency of slow wave: 0.02–20 Hz, fast activity: 20-170 Hz) (Supplementary Fig. S2). Both PAC-Z and PAC-positive rates tended to be high when slow wave frequency was <2 Hz and fast activity frequency was >40 Hz. Therefore, in the next analysis, we focused on a narrower frequency range (central frequency of slow wave: 0.02-2 Hz, fast activity: 50–170 Hz) that showed comparatively high PAC (Supplementary Fig. S3). PAC-Z and the PAC-positive rate seemed to show similar behavior and tended to be higher as sleep deepened, mostly during SWS, while they tended to be lower during REM sleep. PAC-Z was high when the slow wave frequency was 0.3-1.2, 0.3-1.0, 0.2-1.2, and 0.4-1.0 Hz during wakefulness, LS, SWS, and REM sleep, respectively.

The central frequency of the slow wave frequency range that showed high PAC-Z values was 0.5-0.6 Hz in all stages. PAC-Z value was high with fast activity of approximately 90 Hz during wakefulness, LS, and REM sleep, and a wide range of frequencies during SWS.

Posterior region showed high PAC-Z values across all sleep stages, particularly during REM sleep. Next, we sought to elucidate where PAC was enhanced in the brain during each sleep stage. To reveal the spatial dynamics of PAC, we projected the PAC-Z of each sleep stage to 3D-MNI standard space (Supplementary Fig. S4 for individual maps of two patients, and Fig. 2 for averaged maps of all patients). These PAC-Z maps revealed that PAC tended to be distributed widely in the brain at 0.5-0.6 Hz in all stages (Fig. 2). Furthermore, PAC was high over a large area of the brain, particularly during SWS. In addition, we observed that the posterior region, including the TPJ, showed high PAC across all sleep stages, particularly during REM sleep.

Figure 2

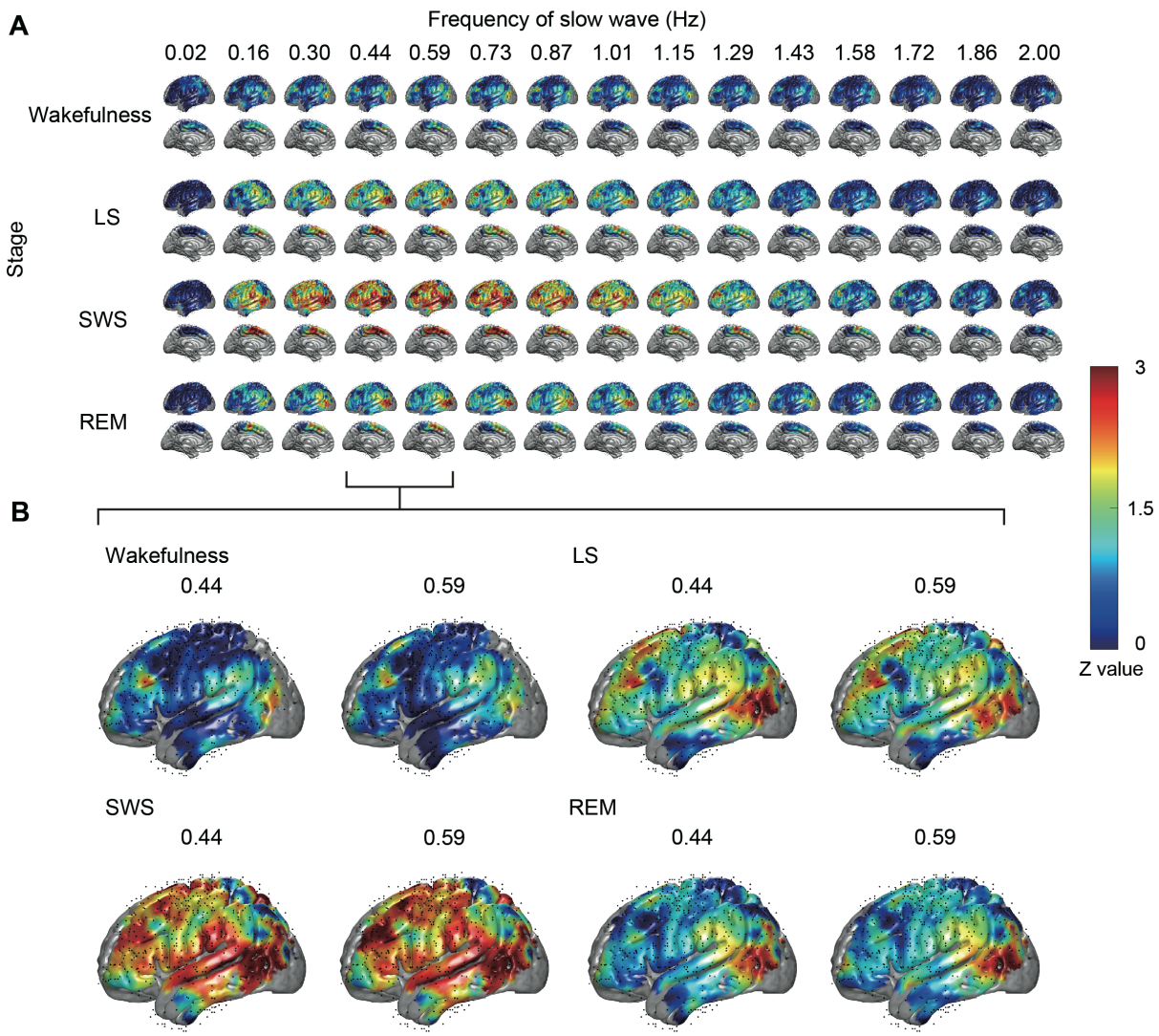

Phase-amplitude coupling (PAC) strength map. PAC-Z values of non-epileptic electrodes of all patients are projected to MNI standard space. It is considered biologically meaningless when a PAC- Z value is negative. Therefore the lowest value of the color bar was set to zero. Areas with z-values greater than 3 are depicted with the same color as 3, and areas with z-values lower than zero are depicted with the same color as zero. **A**) Each column shows PAC-Z strength maps of each slow wave frequency bin (central frequency: 0.02–2 Hz) and each row shows PAC-Z strength maps in each sleep stage (wakefulness, light sleep [LS], slow

wave sleep [SWS], and rapid eye movement [REM] sleep). PAC-Zs of fast activity frequency bins (central frequency: 50–170 Hz) are averaged and shown for each slow wave frequency bin. **B**) Enlarged PAC strength maps with slow wave frequency of 0.44 and 0.59 Hz, which are used in the following statistical analyses. Note that the PAC is high over a large area of the brain during SWS, whereas high PAC is observed in restricted areas, such as the lateral posterior region around the temporo-parieto-occipital junction, during REM sleep and, to a lesser degree, during wakefulness.

Posterior region showed significantly higher PAC-Z value than the frontal region during REM sleep. To test the hypothesis that PAC in the posterior cortical region was significantly enhanced during wakefulness and REM sleep, we delineated two anatomical ROIs, the frontal ROI and posterior ROI (Fig. 3A), and compared the averaged PAC-Z values of channels in each ROI. We found that the PAC-Z in the posterior ROI was significantly higher than that in the frontal ROI during REM sleep ($p=0.004$, Mann-Whitney U test) (Fig. 3B). Additionally, during wakefulness, the PAC-Z value in the posterior ROI tended to be higher than that in the frontal ROI, but this difference was not significant ($p=0.074$, Mann-Whitney U test).

Figure 3

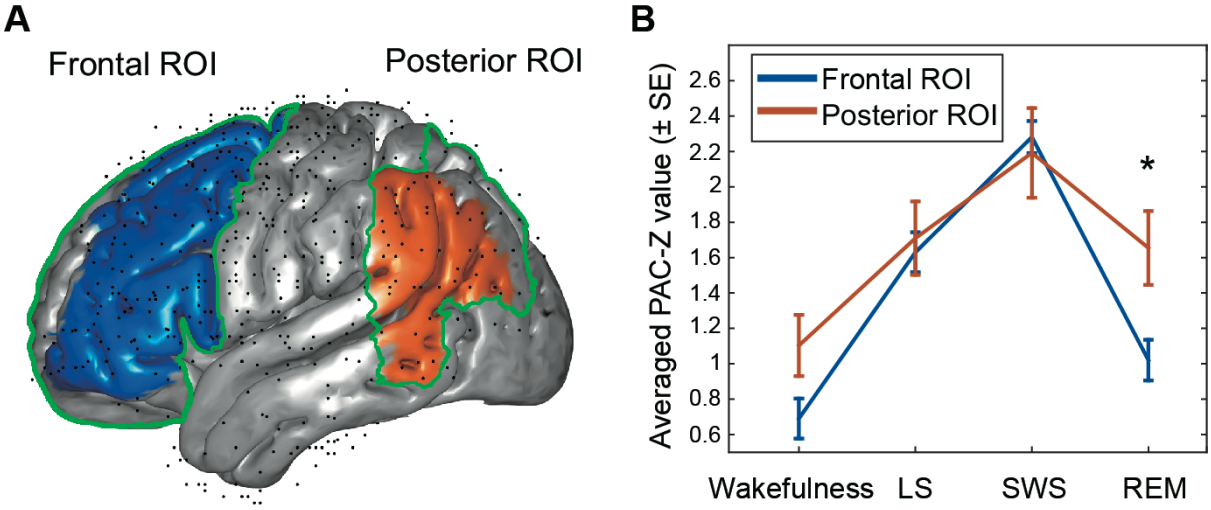

Phase-amplitude coupling (PAC) comparison using anatomical regions of interest (ROIs). **A**) ROIs are anatomically defined as follows: Frontal ROI (blue), the lateral frontal lobe, except for the precentral gyrus; posterior ROI (orange), the temporo-parietal junction. Two ROIs are limited to the voxels that included more than three patients' electrodes within a 15-mm radius. Green lines are edges of the ROIs without this limitation. **B**) Averaged PAC-Z (± standard error [SE]) of electrodes within the frontal ROI and posterior ROI are plotted across four sleep stages. The PAC-Z of electrodes in the posterior ROI is significantly higher than that in the frontal ROI during REM sleep (p=0.004, Mann-Whitney U test) and a similar tendency is observed during wakefulness (p=0.074, Mann-Whitney U test).

Spatial distribution of power did not fully correspond to PAC distribution. We analyzed the power spectra of slow wave and fast activity (Supplementary Fig. S5) in each sleep stage, the power distribution map of slow waves (Supplementary Fig. S6) and fast activity (Supplementary Fig. S7), and compared power in the frontal ROI with that in the posterior ROI in each stage (Supplementary Fig. S8 and S9). Slow wave power showed a peak of approximately 0.6 Hz during SWS, and possibly during LS, whereas fast activity power showed no apparent peak. The peak of slow wave power of approximately 0.6 Hz during LS and SWS was regarded as the power of the slow oscillations that are known to be present during NREM sleep (Timofeev 2000; Dalal *et al.* 2010; Le Van Quyen *et al.* 2010; Nir *et al.* 2011). These results showed that both PAC-Z and slow wave power were high at approximately 0.6 Hz during LS and SWS, while only PAC-Z value, but not slow wave power, was high during wakefulness and REM sleep. The spatial distribution of power did not correspond to that of PAC. Slow wave power was significantly higher in the posterior ROI than in the frontal ROI during SWS ($p=0.003$, Mann-Whitney U test) and REM sleep ($p=0.003$, Mann-Whitney U test; Supplementary Fig. S8). Fast activity power was significantly higher in the posterior ROI than in the frontal ROI only during SWS, with a central frequency of 170 Hz ($p=0.010$, Mann-Whitney U test; Supplementary Fig. S9).

Discussion

In this study, we investigated the spatial distribution of PAC strength during sleep and wakefulness to gain insight into the neurological correlates of consciousness. This study was performed taking full advantage of ECoG, which has high spatiotemporal resolution. We observed PAC between slow waves of 0.5-0.6 Hz and gamma activities, even during wakefulness and REM sleep, although slow oscillation power was not prominent during these stages. We also showed that PAC strength was significantly higher in the posterior region than in the frontal region during REM sleep. It also tended to be higher in the posterior region than in the frontal region during wakefulness, although not statistically significant. PAC is considered to reflect neuronal coding in information processing in the brain (Canolty *et al.* 2006; Handel and Haarmeier 2009; Axmacher *et al.* 2010; Canolty and Knight 2010; Tort *et al.* 2010; Fontolan *et al.* 2014); hence, our findings suggest that the posterior region has some functional role in REM sleep.

Analysis of anatomical ROIs revealed that PAC strength was significantly higher in the posterior ROI than in the frontal ROI during REM sleep and was the highest during SWS

462 in both ROIs (Fig. 3B). Previous sleep studies in humans and monkeys have shown that PAC
463 is mostly prominent in deep NREM sleep, consistent with our results (Takeuchi *et al.* 2015;
464 Amiri *et al.* 2016; von Ellenrieder *et al.* 2020). Cortical slow oscillation has "UP"
465 (depolarization) and "DOWN" (hyperpolarization) states, and it has been reported that
466 gamma oscillation usually occurs during the cortical "UP" state (Steriade 1996; Le Van
467 Quyen *et al.* 2010; Valderrama *et al.* 2012). Although slow oscillations during SWS and their
468 association with gamma activity have been intensively investigated, their physiological roles
469 are yet to be fully understood. Slow waves during SWS occur locally, and travel in the frontal
470 to posterior direction via the cingulate pathway (Massimini *et al.* 2004; Murphy *et al.* 2009).
471 Suppression/enhancement of slow oscillation interferes with/improves memory retention, and
472 slow oscillations are thought to be related to memory consolidation (Marshall *et al.* 2006;
473 Aeschbach *et al.* 2008; Crupi *et al.* 2009; Nir *et al.* 2011).
474 Although PAC is theoretically independent of the amplitude of slow wave and fast
475 activity, changes in amplitude could possibly affect the signal-to-noise ratio of phase and
476 amplitude variables, and thus PAC (Aru *et al.* 2014). To exclude the possibility that PAC was
477 merely the result of a change in amplitude of slow wave and fast activity, we also
478 investigated their power distribution. The logarithm of slow wave power was significantly

479 higher in the posterior ROI than in the frontal ROI during REM sleep and SWS, and that of
480 fast activity was significantly higher in the posterior ROI than in the frontal ROI during SWS
481 only, with a central frequency of 170 Hz (Supplementary Fig. S8 and S9). A recent
482 intracranial EEG study has demonstrated that the frontal lobe showed significantly lower
483 median delta power during N3 (comparable to SWS), wakefulness, and REM sleep, which
484 might be in accordance with our results (von Ellenrieder *et al.* 2020). It should be noted that
485 the power distribution map was not fully consistent with the PAC-Z strength map in our
486 study. The PAC-Z was high in the supramarginal gyrus and angular gyrus, while the power of
487 fast activities or slow waves was not prominent in these regions (Fig. 2, Supplementary Figs.
488 S6 and S7). Therefore, we consider that independent of the amplitudes of fast activities or
489 slow waves, the posterior regions play some functional role via neuronal activities that are
490 reflected by PAC.

491 During NREM sleep (LS and SWS), PAC was prominent for slow waves of 0.5-0.6
492 Hz and gamma activities, and the slow wave power spectrum peaked at approximately 0.6
493 Hz, which leads to the characteristic slow oscillations in NREM sleep. In contrast, during
494 wakefulness and REM sleep, PAC was observed for slow waves of 0.5-0.6 Hz and gamma
495 activities, although the slow wave power spectrum peak was unclear. The relationship of slow

496 wave power and PAC is completely different between NREM sleep and other states

497 (wakefulness or REM sleep). We speculate that PAC during wakefulness or REM sleep has a

498 different physiological role from that during NREM sleep. Our results may support the

499 hypothesis that neural correlates of consciousness, which are defined as the minimum

500 neuronal mechanisms jointly sufficient for any one specific conscious percept (Boly *et al.*

501 2017), are located in the posterior cortical regions. Moreover, to the best of our knowledge,

502 no previous report has shown that PAC may reflect some physiological neuronal phenomenon

503 in that region during REM sleep. Where the neural correlates of consciousness are located in

504 the human brain ("front" or "back") has been a matter of debate (Koch *et al.* 2016; Boly *et al.*

505 2017; Mashour 2018). Clinical and animal studies have suggested that the prefrontal cortex

506 plays a key role in making sensory input conscious, whereas other studies have shown that

507 the posterior cortex is important for consciousness (Del Cul *et al.* 2009; Boly *et al.* 2017; van

508 Vugt 2018). Siclari *et al*. have shown that dreaming experiences are associated with local

509 decreases in delta activity in posterior cortical regions (Siclari *et al.* 2017). They have also

510 shown that the dreaming experience is associated with local increases in gamma activity in

511 the posterior cortical regions, particularly during NREM sleep. They reasoned that as long as

512 the posterior cortical region does not have high delta power, which prevents conscious

experience during sleep, the specific content of experiences is dictated by specific groups of neurons that do and do not fire strongly. They did not investigate the role of PAC. Taking our results into account, slow waves in the posterior cortical region possibly control the degree of consciousness, and moreover, determine which local neuronal group, associated with conscious experience content, will fire via PAC.

From the viewpoint of network theory, Usami *et al*. have revealed that greater neuronal propagation toward the parietal lobe was induced by single-pulse electrical stimulation to the frontal lobe during SWS than during wakefulness. Moreover, they showed that propagation within the parietal lobe elicited by parietal stimulation increased during REM sleep. They concluded that changes in neural propagation across large-scale frontal-parietal networks may contribute to consciousness (or unconsciousness) (Usami *et al.* 2019). Of note, PAC was high in the posterior cortical region during REM sleep in our study, which is characterized by an "activated" EEG pattern containing low amplitude and irregular frequency (Aserinsky and Kleitman 1953; Steriade *et al.* 2001). A previous study has reported that interhemispheric correlations of very slow (<0.1 Hz) fluctuations of neuronal firing rate and gamma local field potential could be seen during sleep and were especially enhanced during stage 2 and REM sleep, suggesting that the correlated spontaneous fluctuations might

530 serve some role in maintenance and renormalization of synaptic contacts in sleep (Nir *et al.*
531 2008). In terms of resting-state functional MRI study, blood oxygenation level dependent
532 signal fluctuated rhythmically with a slow frequency ranging around 0.1 to 0.01 Hz, and
533 default-mode network (DMN) positively correlated with association cortex and negatively
534 correlated with sensorimotor regions during REM sleep (Chow *et al.* 2013). The connectivity
535 between inferior/middle temporal gyrus and DMN core region (e.g. inferior parietal lobe and
536 angular gyrus) has been shown to be stronger during REM sleep than deep NREM
537 sleep (Koike *et al.* 2011). In our study, PAC seemed to be enhanced in the posterior region,
538 particularly in the area close to the TPJ or parietal association cortex, which integrates
539 multimodal sensory information (Eddy 2016; Grivaz *et al.* 2017). Based on the previous
540 findings and our results, it is tempting to speculate that information processing, reflected by
541 PAC, might increase within the posterior region, resulting in dreaming experience during
542 REM sleep, while the other type of global brain PAC and global high-power delta activities
543 during NREM sleep inhibit such vivid experiences.
544 This study has some limitations. PAC and low-frequency power have been reported
545 to be higher in the epileptic regions than in the normal regions, and their positive correlation
546 was found (Amiri *et al.* 2016). Because we eliminated electrodes in SOZ and IZ from PAC

analysis in this study, it is less likely that our result was biased by epileptic background slowing. However, we cannot exclude the possibility that there were non-epileptic regions that did not contain epileptic spikes but did contain epileptic slow waves, which influenced the result. The background of patients varied, including the anti-epileptic drugs used, electrode coverage area, and number of electrodes used, all of which could bias our findings. To resolve these potential biases, we produced time-shifted ECoG data to generate statistical significance, and analyzed the patients as a group, rather than individually.

In summary, we found that PAC strength was higher in the posterior cortical region than in the frontal cortical region during REM sleep. Our results may suggest that PAC in the posterior “hot zone” plays an important physiological role in maintaining dreaming experience.

Conflict of interest:

The authors declare no competing financial interests.

Funding:

This work was supported by Japan Society for the Promotion of Science KAKENHI (grant numbers 15H05874, 15H05875, 18H02709, 18H06087, 18K19514, 19H03574, 19K21210, 20H05471, 20K16492, and 20K21573).

Acknowledgements:

We are grateful to Prof. Toshio Aoyagi, Department of Advanced Mathematical Sciences, Graduate School of Informatics, Kyoto University and Dr. Kohei Nakajima, Graduate School of Information Science and Technology, The University of Tokyo, for helpful discussions. We would like to thank the Academic Center for Computing and Media Studies, Kyoto University, for the use of their supercomputer employed in this research. JT belongs to Department of Respiratory Care and Sleep Control Medicine, which is funded by the endowments from Philips Japan, ResMed Japan, Fukuda Denshi, and Fukuda Lifetech Keiji to Kyoto University. KU, MM, MI, and AI belong to the Department of Epilepsy, Movement Disorders and Physiology, which is an Industry-Academia Collaboration supported by a grant

575 from Eisai Company, NIHON KOHDEN CORPORATION, Otsuka Pharmaceutical Co., and

576 UCB Japan Co., Ltd.

References

Aeschbach D, Cutler AJ, Ronda JM. 2008. A role for non-rapid-eye-movement sleep homeostasis in perceptual learning. J Neurosci. 28:2766-2772.

Amiri M, Frauscher B, Gotman J. 2016. Phase-Amplitude Coupling Is Elevated in Deep Sleep and in the Onset Zone of Focal Epileptic Seizures. Front Hum Neurosci. 10:387.

Aru J, Aru J, Priesemann V, Wibral M, Lana L, Pipa G, Singer W, Vicente R. 2014. Untangling cross-frequency coupling in neuroscience. Curr Opin Neurobiol. 31C:51-61.

Aserinsky E, Kleitman N. 1953. Regularly occurring periods of eye motility, and concomitant phenomena, during sleep. Science. 118:273-274.

Axmacher N, Henseler MM, Jensen O, Weinreich I, Elger CE, Fell J. 2010. Cross-frequency coupling supports multi-item working memory in the human hippocampus. Proc Natl Acad Sci U S A. 107:3228-3233.

Boly M, Massimini M, Tsuchiya N, Postle BR, Koch C, Tononi G. 2017. Are the Neural Correlates of Consciousness in the Front or in the Back of the Cerebral Cortex? Clinical and Neuroimaging Evidence. J Neurosci. 37:9603-9613.

Braun AR. 1997. Regional cerebral blood flow throughout the sleep-wake cycle. An H2(15)O PET study. Brain. 120 (Pt 7):1173-1197.

Buzsaki G, Wang XJ. 2012. Mechanisms of gamma oscillations. Annu Rev Neurosci. 35:203-225.

Canolty RT, Edwards E, Dalal SS, Soltani M, Nagarajan SS, Kirsch HE, Berger MS, Barbaro NM, Knight RT. 2006. High gamma power is phase-locked to theta oscillations in human neocortex. Science. 313:1626-1628.

Canolty RT, Knight RT. 2010. The functional role of cross-frequency coupling. Trends Cogn Sci. 14:506-515.

Chow HM, Horovitz SG, Carr WS, Picchioni D, Coddington N, Fukunaga M, Xu Y, Balkin TJ, Duyn JH, Braun AR. 2013. Rhythmic alternating patterns of brain activity distinguish rapid eye movement sleep from other states of consciousness. Proc Natl Acad Sci U S A. 110:10300-10305.

Crupi D, Hulse BK, Peterson MJ, Huber R, Ansari H, Coen M, Cirelli C, Benca RM, Ghilardi MF, Tononi G. 2009. Sleep-Dependent Improvement in Visuomotor Learning: A Causal Role for Slow Waves. Sleep. 32:1273-1284.

Dalal SS, Hamamé CM, Eichenlaub JB, Jerbi K. 2010. Intrinsic coupling between gamma oscillations, neuronal discharges, and slow cortical oscillations during human slow-wave sleep. J Neurosci. 30:14285-14287.

Del Cul A, Dehaene S, Reyes P, Bravo E, Slachevsky A. 2009. Causal role of prefrontal cortex in the threshold for access to consciousness. Brain. 132:2531-2540.

Eddy CM. 2016. The junction between self and other? Temporo-parietal dysfunction in neuropsychiatry. Neuropsychologia. 89:465-477.

Fontolan L, Morillon B, Liegeois-Chauvel C, Giraud AL. 2014. The contribution of frequency-specific activity to hierarchical information processing in the human auditory cortex. Nat Commun. 5:4694.

Fries P. 2005. A mechanism for cognitive dynamics: neuronal communication through neuronal coherence. Trends Cogn Sci. 9:474-480.

Grivaz P, Blanke O, Serino A. 2017. Common and distinct brain regions processing multisensory bodily signals for peripersonal space and body ownership. Neuroimage. 147:602-618.

Handel B, Haarmeier T. 2009. Cross-frequency coupling of brain oscillations indicates the success in visual motion discrimination. Neuroimage. 45:1040-1046.

He BJ, Zempel JM, Snyder AZ, Raichle ME. 2010. The temporal structures and functional significance of scale-free brain activity. Neuron. 66:353-369.

Hobson JA. 2009. REM sleep and dreaming: towards a theory of protoconsciousness. Nat Rev

Neurosci. 10:803-813.

Koch C, Massimini M, Boly M, Tononi G. 2016. Neural correlates of consciousness: progress and problems. Nat Rev Neurosci. 17:307-321.

Koike T, Kan S, Misaki M, Miyauchi S. 2011. Connectivity pattern changes in default-mode network with deep non-REM and REM sleep. Neurosci Res. 69:322-330.

Le Van Quyen M, Staba R, Bragin A, Dickson C, Valderrama M, Fried I, Engel J. 2010. Large-scale microelectrode recordings of high-frequency gamma oscillations in human cortex during sleep. J Neurosci. 30:7770-7782.

Marshall L, Helgadottir H, Molle M, Born J. 2006. Boosting slow oscillations during sleep potentiates memory. Nature. 444:610-613.

Mashour GA. 2018. The controversial correlates of consciousness. Science. 360:493-494.

Massimini M, Huber R, Ferrarelli F, Hill S, Tononi G. 2004. The sleep slow oscillation as a traveling wave. J Neurosci. 24:6862-6870.

Matsumoto R, Imamura H, Inouchi M, Nakagawa T, Yokoyama Y, Matsuhashi M, Mikuni N, Miyamoto S, Fukuyama H, Takahashi R, Ikeda A. 2011. Left anterior temporal cortex actively engages in speech perception: A direct cortical stimulation study. Neuropsychologia. 49:1350-1354.

Matsumoto R, Nair DR, LaPresto E, Najm I, Bingaman W, Shibasaki H, Luders HO. 2004. Functional connectivity in the human language system: a cortico-cortical evoked potential study. Brain. 127:2316-2330.

Motoi H, Miyakoshi M, Abel TJ, Jeong JW, Nakai Y, Sugiura A, Luat AF, Agarwal R, Sood S, Asano E. 2018. Phase-amplitude coupling between interictal high-frequency activity and slow waves in epilepsy surgery. Epilepsia. 59:1954-1965.

Murphy M, Riedner BA, Huber R, Massimini M, Ferrarelli F, Tononi G. 2009. Source modeling sleep slow waves. Proc Natl Acad Sci U S A. 106:1608-1613.

Nakae T, Matsumoto R, Kunieda T, Arakawa Y, Kobayashi K, Shimotake A, Yamao Y, Kikuchi T, Aso T, Matsuhashi M, Yoshida K, Ikeda A, Takahashi R, Lambon Ralph MA, Miyamoto S. 2020. Connectivity Gradient in the Human Left Inferior Frontal Gyrus: Intraoperative Cortico-Cortical Evoked Potential Study. Cereb Cortex. 30:4633-4650.

Nir Y, Mukamel R, Dinstein I, Privman E, Harel M, Fisch L, Gelbard-Sagiv H, Kipervasser S, Andelman F, Neufeld MY, Kramer U, Arieli A, Fried I, Malach R. 2008. Interhemispheric correlations of slow spontaneous neuronal fluctuations revealed in human sensory cortex. Nat Neurosci. 11:1100-1108.

Nir Y, Staba RJ, Andrillon T, Vyazovskiy VV, Cirelli C, Fried I, Tononi G. 2011. Regional slow

waves and spindles in human sleep. Neuron. 70:153-169.

Nonoda Y, Miyakoshi M, Ojeda A, Makeig S, Juhasz C, Sood S, Asano E. 2016. Interictal high-frequency oscillations generated by seizure onset and eloquent areas may be differentially coupled with different slow waves. Clin Neurophysiol. 127:2489-2499.

Palmini A, Najm I, Avanzini G, Babb T, Guerrini R, Foldvary-Schaefer N, Jackson G, Luders HO, Prayson R, Spreafico R, Vinters HV. 2004. Terminology and classification of the cortical dysplasias. Neurology. 62:S2-8.

Rechtschaffen A, Kales A. 1968. A manual of standardized terminology, techniques and scoring system for sleep stages of human subjects: Los Angeles (Calif.) : University of California. Brain research institute.

Schurz M, Tholen MG, Perner J, Mars RB, Sallet J. 2017. Specifying the brain anatomy underlying temporo-parietal junction activations for theory of mind: A review using probabilistic atlases from different imaging modalities. Hum Brain Mapp. 38:4788-4805.

Siclari F, Baird B, Perogamvros L, Bernardi G, LaRocque JJ, Riedner B, Boly M, Postle BR, Tononi G. 2017. The neural correlates of dreaming. Nat Neurosci. 20:872-878.

Steriade M. 1996. Synchronization of fast (30-40 Hz) spontaneous cortical rhythms during brain activation. J Neurosci. 16:392-417.

Steriade M, Timofeev I, Grenier F. 2001. Natural waking and sleep states: a view from inside neocortical neurons. J Neurophysiol. 85:1969-1985.

Takeuchi S, Mima T, Murai R, Shimazu H, Isomura Y, Tsujimoto T. 2015. Gamma Oscillations and Their Cross-frequency Coupling in the Primate Hippocampus during Sleep. Sleep. 38:1085-1091.

Timofeev I. 2000. Origin of slow cortical oscillations in deafferented cortical slabs. Cereb Cortex. 10:1185-1199.

Tort AB, Komorowski R, Eichenbaum H, Kopell N. 2010. Measuring phase-amplitude coupling between neuronal oscillations of different frequencies. J Neurophysiol. 104:1195-1210.

Tort AB, Komorowski RW, Manns JR, Kopell NJ, Eichenbaum H. 2009. Theta-gamma coupling increases during the learning of item-context associations. Proc Natl Acad Sci U S A. 106:20942-20947.

Tort ABL. 2008. Dynamic cross-frequency couplings of local field potential oscillations in rat striatum and hippocampus during performance of a T-maze task. Proc Natl Acad Sci U S A. 105:20517-20522.

Usami K, Korzeniewska A, Matsumoto R, Kobayashi K, Hitomi T, Matsuhashi M, Kunieda T,

Mikuni N, Kikuchi T, Yoshida K, Miyamoto S, Takahashi R, Ikeda A, Crone NE. 2019. The neural tides of sleep and consciousness revealed by single-pulse electrical brain stimulation. Sleep. 42.

Valderrama M, Crepon B, Botella-Soler V, Martinerie J, Hasboun D, Alvarado-Rojas C, Baulac M, Adam C, Navarro V, Le Van Quyen M. 2012. Human gamma oscillations during slow wave sleep. PLoS One. 7:e33477.

van Vugt B. 2018. The threshold for conscious report: Signal loss and response bias in visual and frontal cortex. Science. 360:537-542.

von Ellenrieder N, Gotman J, Zelmann R, Rogers C, Nguyen DK, Kahane P, Dubeau F, Frauscher B. 2020. How the Human Brain Sleeps: Direct Cortical Recordings of Normal Brain Activity. Ann Neurol. 87:289-301.

von Stein A, Sarnthein J. 2000. Different frequencies for different scales of cortical integration: from local gamma to long range alpha/theta synchronization. Int J Psychophysiol. 38:301-313.

Wieser HG, Blume WT, Fish D, Goldensohn E, Hufnagel A, King D, Sperling MR, Luders H, Pedley TA. 2001. ILAE Commission Report. Proposal for a new classification of outcome with respect to epileptic seizures following epilepsy surgery. Epilepsia. 42:282-286.

Wood JN, Grafman J. 2003. Human prefrontal cortex: processing and representational

713 perspectives. Nat Rev Neurosci. 4:139-147.

714